

Intrinsic Organic Semiconductors as Hole Transport Layers in p–i–n Perovskite Solar Cells

Isidora Susic, Kassio P. S. Zanoni, Abhyuday Paliwal, Ismail C. Kaya, Zafer Hawash,* Michele Sessolo,* Ellen Moons, and Henk J. Bolink

Thin polymeric and small-molecular-weight organic semiconductors are widely employed as hole transport layers (HTLs) in perovskite solar cells. To ensure ohmic contact with the electrodes, the use of doping or additional high work function (WF) interlayer is common. In some cases, however, intrinsic organic semiconductors can be used without any additive or buffer layers, although their thickness must be tuned to ensure selective and ohmic hole transport. Herein, the characteristics of thin HTLs in vacuum-deposited perovskite solar cells are studied, and it is found that only very thin (<5 nm) HTLs readily result in high-performing devices, as the HTL acts as a WF enhancer while still ensuring selective hole transfer, as suggested by ultraviolet photoemission spectroscopy and Kelvin probe measurements. For thicker films (≥ 5 nm), a dynamic behavior for consecutive electrical measurements is observed, a phenomenon which is also common to other widely used HTLs. Finally, it is found that despite their glass transition temperature, small-molecule HTLs lead to thermally unstable solar cells, as opposed to polymeric materials. The origin of the degradation is still not clear, but might be related to chemical reactions/diffusion at the HTL/perovskite interface, in detriment of the device stability.

1. Introduction


In the past decade, hybrid organic–inorganic perovskite solar cells attracted considerable attention due to their optoelectronic properties, such as high absorption coefficient, low exciton binding energy, high charge carrier mobility, and widely tunable bandgap.^[1–3] Although the record efficiency of perovskite solar cells has exceeded 25%,^[4,5] there are still challenges to be overcome for their commercialization, in particular, the device's long-term stability and the development of scalable and reliable fabrication methods.^[6,7] In general, perovskite solar cells include a transparent electrode, a perovskite film sandwiched between selective hole transport layers (HTLs) and electron transport layers (ETLs), and a (metallic) counter electrode. Depending on which layer is deposited on the transparent substrates, the device can be built in two configurations of opposite polarity, namely n–i–p and p–i–n, where the transparent conductive substrate is coated with the ETL or the HTL, respectively.^[8–10] The ideal hole transport material (HTM) should be thermally and chemically stable, have high hole mobility, and matched electronic energy levels with the perovskite absorber, to efficiently and selectively transport the photogenerated charge carriers to the electrode.^[11–14] To date, 2,2',7,7'-tetrakis(*N,N*-di-*p*-methoxyphenylamino)-9,9'-spirobifluorene (spiro-OMeTAD) is the most studied and widely used HTM in n–i–p perovskite solar cells.^[9,15] In p–i–n devices, the variety of possible HTMs is much larger, but the most common are poly[bis(4-phenyl)(2,4,6-trimethylphenyl)amine] (PTAA) and the inorganic p-type semiconductor NiO_x.^[16–20]

When using low-molecular-weight organic semiconductors (small molecules) as the HTL, an additional interlayer is often used to increase the work function (WF) of the indium tin oxide (ITO) and ensure ohmic charge injection/collection.^[21] Common materials are organic semiconductors with high WF, such as 2,2'-(perfluoronaphthalene-2,6-diylidene) dimalononitrile (F₆-TCNNQ), doped layers, or high WF metal oxides, in particular, MoO₃, W₂O₃, and V₂O₅.^[22–25] MoO₃ is widely adopted as it can be easily sublimed, and its high WF induces a density of free positive charges at the interface with organic semiconductors.^[26,27] This is typically attained through annealing of the MoO₃/HTL bilayer, resulting in ohmic charge transport.^[28] It

I. Susic, K. P. S. Zanoni, A. Paliwal, I. C. Kaya, M. Sessolo, H. J. Bolink
Instituto de Ciencia Molecular
Universidad de Valencia
C/ Catedrático J. Beltrán 2, 46980 Paterna, Spain
E-mail: michele.sessolo@uv.es

I. C. Kaya
Department of Metallurgical and Materials Engineering
Konya Technical University
42250 Konya, Turkey

Z. Hawash,^[†] E. Moons
Department of Engineering and Physics
Karlstad University
SE-65188 Karlstad, Sweden
E-mail: zhawash@birzeit.edu

 The ORCID identification number(s) for the author(s) of this article can be found under <https://doi.org/10.1002/solr.202100882>.

^[†]Present address: Department of Physics, Birzeit University, 71939 Birzeit, Palestine.

© 2021 The Authors. Solar RRL published by Wiley-VCH GmbH. This is an open access article under the terms of the Creative Commons Attribution License, which permits use, distribution and reproduction in any medium, provided the original work is properly cited.

DOI: 10.1002/solr.202100882

is known, however, that the HTL/MoO₃ interface is thermally unstable towards elevated temperatures and ambient light^[29] so that it might undermine the device stability. Such interlayers are not usually needed in combination with polymer HTLs, such as PTAA when they are used in p-i-n solar cells between the ITO and the perovskite film. This is possible thanks to the use of very thin films (<20 nm) and brings the advantage of suppressing interfacial recombination due to the absence of doping.^[30–32] Dopant-free HTLs have been applied in p-i-n solar cells with the perspective of reducing shunts and surface recombination, especially when compared to p-type conducting polymers.^[33,34] Reduction of these non-radiative recombination losses led to the demonstration of record high voltages in p-i-n perovskite solar cells.^[35,36] A recent trend for p-i-n solar cells is the use of self-assembly monolayers (SAMs),^[37,38] which ensure conformal coverage, energy level matching, and suppression of interface recombination.

These materials have also been studied in solar cells employing perovskites prepared by vacuum deposition, a method which is increasingly adopted in view of the advantages of conformal coating, thickness control, compatibility with multilayer devices, such as tandem solar cells, and for being established in several industrial applications.^[39–41] Small molecules, polymers, and SAMs have been extensively studied as HTLs in vacuum-deposited p-i-n perovskite solar cells, reaching power conversion efficiency (PCE) exceeding 20%.^[24,42,43] Recently, Abzieher et al. showed the advantage of using organic semiconductors as substrates for the vacuum processing of methylammonium lead iodide (MAPI) films.^[44] The hydrophobic surface of organics favors the crystallization and orientation of the perovskite film, as opposed to polar metal oxide surfaces, confirming previous observations.^[45–47] Interestingly, they found that a very thin (<3 nm) undoped film of 2,2',7,7'-tetra(*N,N*-di-*p*-tolyl)amino-9,9-spirobifluorene (Spiro-TTB) can be employed to ensure ohmic contact between ITO and the MAPI absorber layer, leading to very efficient solar cells. Another recent report used a thin (<10 nm) film of a fluorinated analog of Spiro-OMeTAD (Spiro-*mF*), to prepare efficient, fully vacuum-deposited perovskite solar cells without any dopant or interlayer at the ITO contact.^[48]

Despite the widespread adoption of intrinsic organic semiconductors as thin HTLs in between the ITO and the perovskite, their thickness-dependent working mechanism and the ohmic hole transport, despite mismatched energy levels with ITO, are not yet clear. In this work, we study in detail the properties of undoped HTLs in fully vacuum-deposited perovskite solar cells, without employing high WF interlayers. We confirm that the HTL thickness plays a key role in the solar cell functioning, dictating the device fill factor (FF). Also, we observe a dynamic behavior in their electrical characteristics, something that is general and common to other thin p-type materials, even polymers such as PTAA. Ultraviolet photoelectron spectroscopy (UPS) was implemented to evaluate energy levels' evolution of the HTLs and was combined with contact potential difference (CPD) measurements using Kelvin Probe (KP) in an inert atmosphere to avoid common pitfalls in evaluating energy levels using UPS only. Thin HTLs act as WF modifiers of the ITO contact, ensuring selective hole extraction thanks to their wide bandgaps. In spite of the simpler fabrication and high PCE, solar cells with thin HTLs of small molecules are found to be thermally unstable,

as opposed to those employing polymers such as PTAA. We exclude the role of the glass transition temperature (T_g) and temperature-induced aggregation of the HTLs in the thermal degradation of the solar cells, which might be guided by other mechanisms, such as exchange and reaction of molecular species between the HTL and the perovskite absorber.

2. Results and Discussion

We fabricated fully vacuum-deposited p-i-n perovskite solar cells with the layout displayed in Figure 1a. The scanning electron microscopy (SEM) images of as-deposited MAPI films (Figure S1, Supporting Information) show a compact morphology composed of small grains (<400 nm in diameter), a common feature of vacuum-deposited perovskite solar cells.^[39] The X-ray diffraction (XRD) pattern of an as-deposited MAPI film is also reported in Figure S1 in the Supporting Information, together with individual whole-pattern fit and reference Bragg's reflections. As previously observed by us and others, co-evaporated MAPI films crystallize in a cubic perovskite phase at room temperature (space group *Pm-3m*), with only a minor contribution from a residual PbI₂ phase.^[44,49] Devices were prepared on ITO-coated glass substrates with the following device configuration: HTL (x nm)/MAPI (500 nm)/C60 (25 nm)/BCP (8 nm)/Ag (100 nm) where BCP is bathocuproine and the HTL is *N*₄,*N*₄,*N*₄'',*N*₄''-tetra([1,1'-biphenyl]-4-yl)-[1,1':4',1''-terphenyl]-4,4''-diamine (TaTm), with thickness varying from 2 to 10 nm. Details of the device fabrication are reported in the Experimental Section.

The current density versus voltage (J - V) curves under simulated solar illumination for p-i-n solar cells with increasing TaTm thickness are reported in Figure 1b. In the absence of a high WF interlayer, such as MoO₃ or F₆-TCNNQ,^[25,50] the J - V curve for the device with 10 nm thick TaTm layer shows a low FF (70–72%), with a slightly s-shaped J - V curve and increased series resistance (reduced slope of the J - V curve around the open-circuit voltage, V_{oc}), which can be ascribed to the mismatch of energy levels between the WF of the ITO and the ionization energy (IE) of TaTm.^[24] The V_{oc} and short circuit current density (J_{sc}) for the same device type are 1090 mV and 21.5 mA cm⁻², respectively. Interestingly, when reducing the TaTm thickness to 5 and further to 2 nm, the FF is increased to >77%, while V_{oc} and J_{sc} are essentially unvaried, resulting in a PCE of approximately 18%, with negligible J - V hysteresis. It is worth noting that as-prepared devices including such thin HTLs show different current-voltage characteristics during the first scans. On the one hand, solar cells with 2 nm thick TaTm layers have high FF and V_{oc} immediately in the first scan, and the J - V curves from consecutive measurements are unaltered (Figure 1c). On the other hand, for devices including a 5 nm thick TaTm layer (Figure 1d), the first J - V scan shows low FF and V_{oc} , which gradually increase with consecutive J - V scans (Figure 1e–f). Only after 3–4 J - V measurements, electrical characteristics stabilize and devices with high rectification and performance (PCE = 18.1 ± 0.4%, Figure 1f) are obtained. As this effect is not observed in solar cells with high WF interlayers at the ITO/HTL interface, it must originate from the energy level mismatch between the ITO WF and the TaTm IE. When a device with

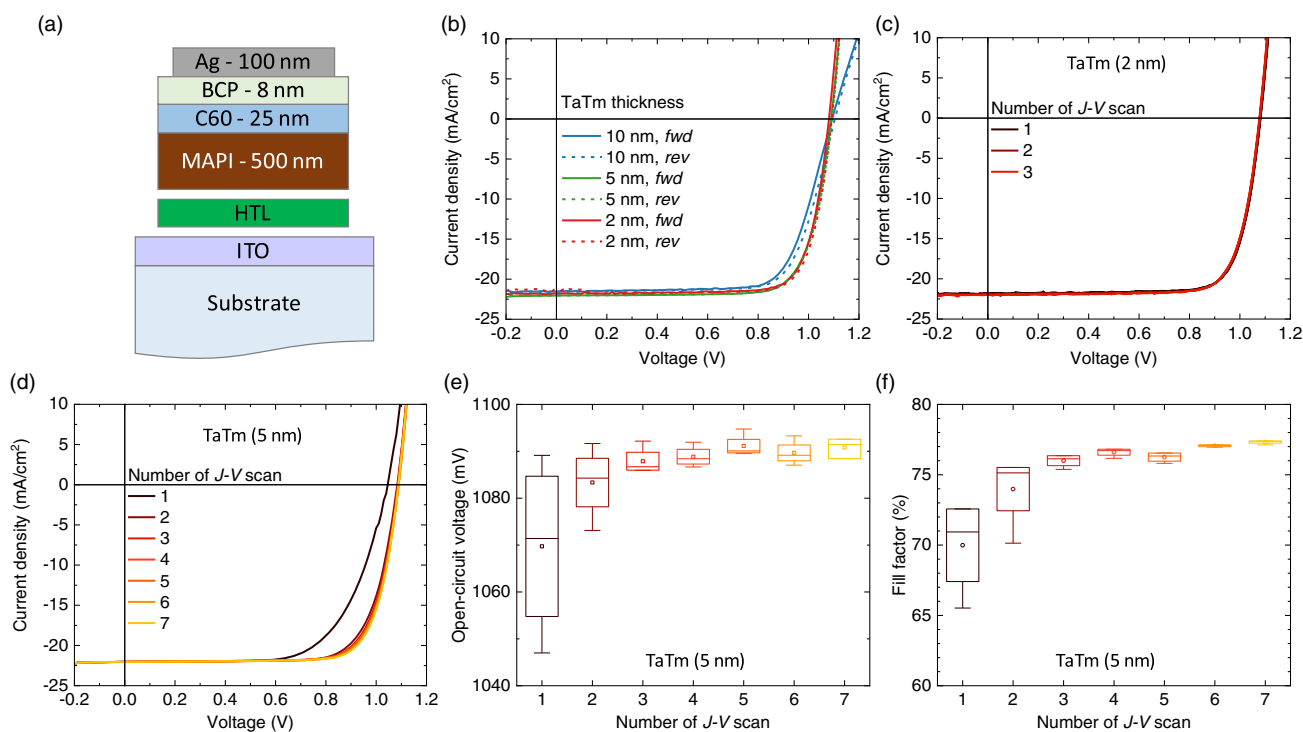


Figure 1. a) Layout of p–i–n solar cells used in this study. b) *J–V* curves under simulated solar illumination for perovskite solar cells with varying TaTm thickness. Solid lines correspond to forward scans (from short to open circuit), and dots to reverse scans (from open to short circuit). Consecutive *J–V* measurement for an as-prepared solar cell employing c) 2 nm thick TaTm and d) 5 nm thick TaTm as the HTL. For the latter, the evolution of the most relevant photovoltaic (PV) parameters is also presented: e) V_{oc} and f) FF.

the same architecture is measured with continuous maximum power point (MPP) tracking under simulated solar illumination, the same dynamic behavior is observed, and the PCE slowly rises in the first 15 min before stabilizing at the maximum value (Figure S3, Supporting Information). The same electrical behavior was observed by using a light-emitting diode (LED) solar simulator with UV component,^[51] as well as with a halogen lamp, with virtually no UV component. No differences were observed, suggesting that the light spectrum is not playing an important role in the device activation.

To promote hole extraction without using reactive high WF compounds, we tested the effect of using a thin film of an organic semiconductor with high IE as an interlayer at the ITO/TaTm interface. Wetzelaer et al. demonstrated that ohmic hole contacts can be easily formed by employing high IE organics placed between an electrode and a semiconductor.^[23] We employed thin (1 and 5 nm) films of tris(4-carbazoyl-9-ylphenyl)amine (TcTa), in view of its reported IE of approximately 5.7–5.8 eV. We initially tested solar cells with p-contact of the type ITO/TcTa (x nm)/TaTm (10 nm) varying the TcTa thickness and using 10 nm thick TaTm, as typically employed in combination with high WF materials, such as MoO₃. The *J–V* curves under illumination (Figure S4, Supporting Information) show that charge extraction in these devices is severely hindered, with a pronounced s-shaped curve independent of the thickness of TcTa employed. This indicates that TcTa is not capable of reducing the hole injection barrier at the ITO/TaTm (10 nm) interface. We further tested devices with the same p-type contact, ITO/TcTa (x nm)/

TaTm, again varying the TcTa thickness, but with a reduced TaTm thickness of 5 nm. In this case, we observed a dependence of the *J–V* curves on the TcTa thickness (Figure 2). In particular, an S-shaped curve is observed for the device with TcTa (5 nm)/TaTm (5 nm) contact, while the diode rectification was found to improve substantially with thinner (2 and 1 nm) TcTa interlayers. Both J_{sc} and V_{oc} are almost unvaried among this device set, and the device behavior is dictated by the FF, which decreases from 76% to 70% and 48% for TcTa thicknesses of 1, 2, and 5 nm, respectively. For solar cells with p-type contact TcTa (1 nm)/TaTm (5 nm), PCE of $18.4 \pm 0.5\%$ was obtained, which is slightly higher compared to the devices without TcTa, which showed a lower V_{oc} . However, the use of TcTa interlayer does not provide a net benefit to the device functioning, as the devices with thin TaTm or thin TcTa/TaTm bilayers show very similar performance.

Also for these solar cells with TcTa/TaTm bilayers, we observed a dynamic behavior in their *J–V* characteristics under illumination (Figure S5, Supporting Information), with the FF increasing from <70% in the first scan to >75% after five *J–V* scans. The photovoltage was observed to be low only in the first measurement, and stabilized at approximately 1090 mV for the following scans.

In order to shed light on the electronic energy levels at these ITO/HTL interfaces, they were studied with a combination of UPS and KP. The full UPS spectra of the highest occupied molecular orbitals (HOMO) for ITO/HTL samples for both TaTm, TcTa, and their bilayer at increasing thickness are reported in

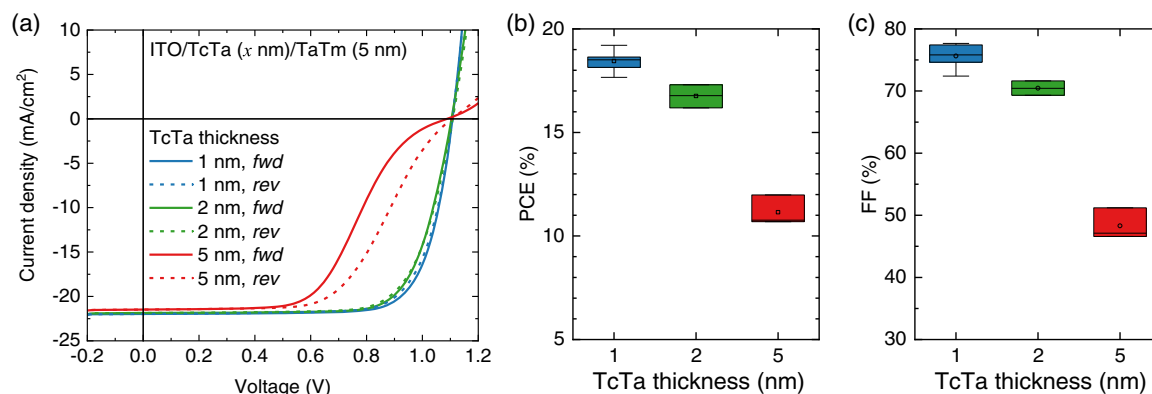


Figure 2. a) J - V curves under simulated solar illumination for perovskite solar cells with p-type contact ITO/TcTa/TaTm (5 nm) and increasing TcTa thickness. Solid lines correspond to forward scans (from short to open circuit), and dots to reverse scans (from open to short circuit). The thickness dependence of the most relevant PV parameters for the same devices is also reported: b) PCE and c) FF.

Figure S6 in the Supporting Information. It is important to notice that during the UPS measurements, we observed a systematic shift of the WF (extracted from the secondary electron cut-off (SECO)) with a consecutive number of collected spectra (Figure S7, Supporting Information), a shift which cannot be ascribed to sample charging. In the case of charging, a similar shift should be observed also for consecutive spectra of the HOMO region, which was not the case in our measurements. It was reported previously that the UV light used in UPS can induce large shifts in the WF of ITO.^[52] As we are measuring rather thin layers of only a few nanometers that are deposited directly on ITO, such effects might take place. Alternatively, the WF of the ITO/organic semiconductor could change under UV irradiation. To avoid this potential problem, we have additionally measured the samples by KP, with which we obtained a precise and stable estimation of the sample WF (Figure 3a). Hence, we estimated the IE and WF of the organic films in two different ways: 1) by extrapolation of the IE from the first scan of the UPS HOMO region on linear scale, and using the WF estimated from the first scan of the UPS cutoff region; and 2) by extrapolation from the UPS HOMO region in semi-log scale (taking into account unwanted emission satellites of He-I by mathematical subtraction) and using the WF obtained by KP. The first method is widely adopted to characterize organic semiconductors, however, the exposure of such samples to ultra-high vacuum (UHV) and ultraviolet light during the UPS measurement can induce changes in the extracted WF values. This is particularly important for thin organic layers on ITO, and other wide bandgap transparent oxides. KP measurements of the WF are done in the dark in an N_2 -filled glovebox, and samples are not perturbed during the measurement. However, the WF value determined by KP is subject to the calibration of the reference probe WF, using a highly oriented pyrolytic graphite (HOPG) sample with a known WF. Other differences between the WF determined by KP and UPS are that UPS measures the lowest value of the WF (cut-off of secondary electrons with the lowest kinetic energy reaching the detector), while KP measures an average value over the area defined by the size (few mm^2) of the reference probe.

In Figure 3, the UPS spectra in the SECO region, the linear spectra at the HOMO edge, and the semi-log spectra at the HOMO edge, together with the corresponding IE interpolation, are reported for TaTm, TcTa, and TcTa/TaTm bilayers as a function of thickness. To help the discussion, the data collected by UPS and KP are summarized in an energy level diagram (Figure 4) where we show 1) the WF as obtained by KP and the IE from semi-log UPS spectra; and 2) the WF as obtained by UPS and the IE extrapolated from linear UPS signal at HOMO edge (all UPS SECO are considered at first scan). UPS gives smaller WF as compared to KP,^[53] especially in the case of ITO and for the thinner TaTm films (2 and 5 nm thick).^[52] In contrast, the WF values extracted from the two methods are similar for 10 nm thick TaTm layers and for the TcTa samples, irrespective of their thickness. We believe the dataset as referred to the WF collected by KP to be more reliable, in view of several considerations: 1) the signal shift observed by UPS in SECO region; 2) the potentially detrimental UHV and UV radiations required for UPS measurement; 3) the use of ITO substrates (which shows unrealistic WF when measured using UPS) to mimic real devices; 4) the fact that SECO in UPS undermines the larger WF values (only the lowest WF is measured); and 5) the WF measured by KP is an averaged WF under the area of the probe. Hence, for the following discussion, we will use the WF extracted from KP and the IE estimated from the semi-log SECO from UPS.

In general, one can observe how all the HTL series show an increased WF with respect to bare ITO (4.29 eV). For example, by depositing TaTm, the WF is increased to 4.63 and 4.68 eV for thicknesses of 2 and 5 nm, respectively. The ITO/TaTm (10 nm) samples showed a lower WF of 4.38 eV, closer to the one of ITO. As the IE varies only slightly for the TaTm thickness series, these data suggest that thin (2 and 5 nm) TaTm layers introduce a surface dipole (pointing outward from the surface, i.e., its negative pole pointing toward TaTm and its positive pole toward ITO), increasing the electrode WF and hence favoring hole injection/extraction.^[54,55] The reduced WF (4.38) for the thicker film (10 nm) suggests that at this thickness the surface properties of the materials resemble more its bulk, as the E_F for TaTm assumes an intrinsic semiconductor would be at

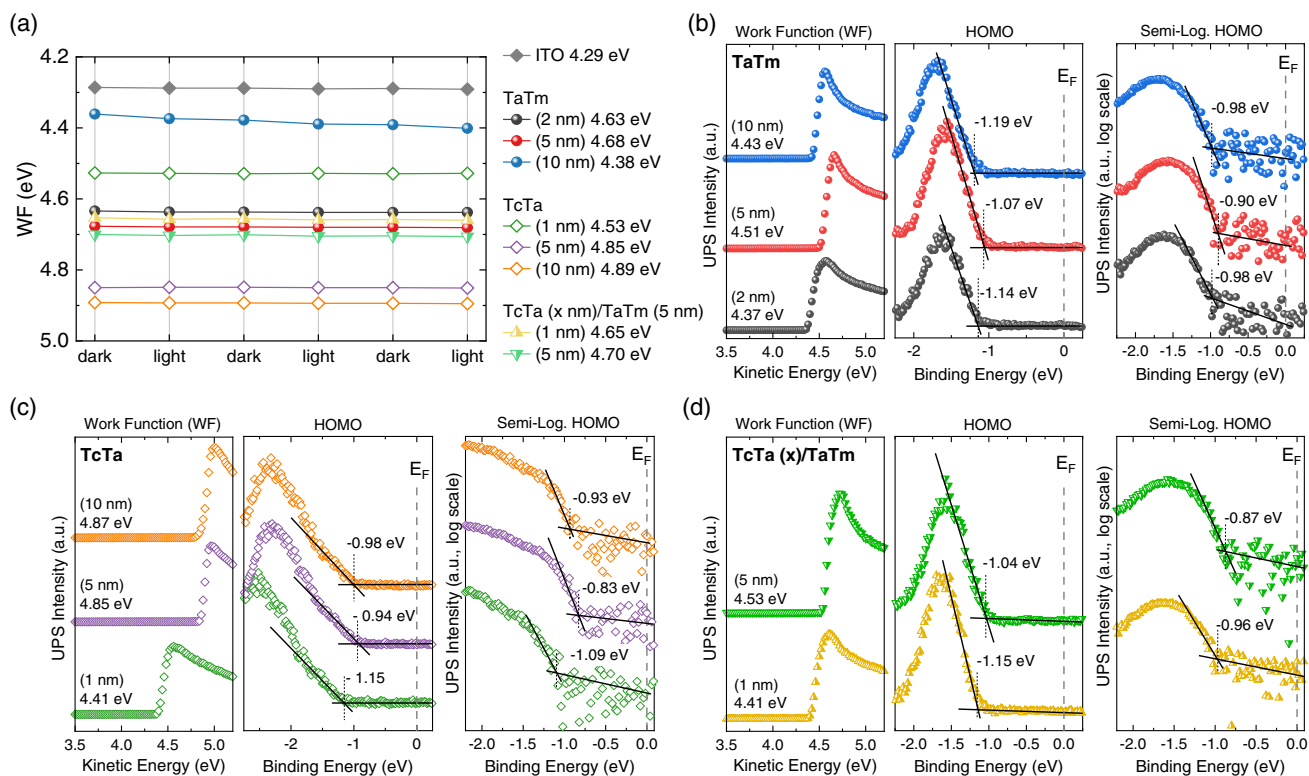


Figure 3. a) WF as obtained from KP measurements for the entire series of HTLs. Measurements were carried out in a nitrogen atmosphere over time to evaluate the signal stability, both in the dark and under illumination to check the signal stability. UPS spectra at the SECO and HOMO regions, the latter both in linear and semi-log scale, for b) TaTm (2–10 nm), c) TcTa (1–10 nm), and d) TcTa/TaTm (5 nm) bilayers (with 1 and 5 nm thick TcTa interlayers). All samples are sublimed on glass/ITO substrates.

approximately 4 eV.^[24] Regarding the IE of TaTm, we obtained a value of 5.62 eV using the standard linear interpolation, and a value of 5.4 eV when using the KP WF and the IE calculated from semi-log UPS spectra. The value of 5.4 eV is close to the expected IE for an arylamine derivative (as α -NPD, N,N' -Bis(naphthalen-1-yl)- N,N' -bis(phenyl)-2,2'-dimethylbenzidine, for example),^[26] and matches also the reported value of the MAPI IE. However, in the case of the bulk TaTm sample (10 nm), we observed an unexpected continuous increase in KP WF value (Figure 3a) as well as a counterintuitively larger WF value as measured by UPS compared to KP (Figure 4), which suggests that TaTm might undergo reactions during UPS measurements.

The deposition of a 1 nm thick TcTa film on ITO increased the WF from 4.29 to 4.53 eV, in a similar fashion to that observed for thin TaTm film. However, the change in WF for 5 and 10 nm thick films deposited on ITO is larger, up to 4.85 and 4.89 eV, respectively. No substantial differences were observed in WF obtained from UPS and KP measurements in the case of TcTa. We observed small changes in the IE as obtained from linear or semi-log interpolation: again, the IE values for the 10 nm thick TcTa film calculated from KP and semi-log interpolation match the literature value of 5.8 eV,^[23] although the difference here between the values extracted from the two methods is very small. As opposed to what was observed for TaTm, in general, the IE of TcTa becomes lower for thinner films.

Regarding the TcTa (x nm)/TaTm (5 nm) bilayers, their WF is close in energy to that of the single 5 nm thick TaTm film, with

values of 4.65 and 4.70 eV for 1 and 5 nm thick TcTa interlayers, respectively. This indicates that TaTm is capable of screening the underlying TcTa film. To discuss the properties of the HTLs in our perovskite solar cells, we should consider an IE (valence band (VB) edge) for MAPI of approximately 5.4 eV,^[56] although recent measurements place it at about 5.2 eV, due to the low density of states at the VB maximum for this semiconductor.^[57] When used in solar cells, the IE of TaTm is well aligned with the VB edge of MAPI, ensuring selective hole extraction without voltage loss. However, the energy mismatch between the underlying ITO WF and the TaTm IE introduces an energy barrier, which hinders hole injection/extraction, resulting in increased series resistance of the solar cell (slope of the J - V curves in Figure 1b). When the layer is sufficiently thin (≤ 5 nm), the material effectively enhances the electrode WF, and its IE is also increased by approximately 0.2 eV, which confirms the presence of an interface dipole. The latter observation indicates an energy mismatch with both the ITO WF and the perovskite VB edge (IE); this is indeed the case in our solar cells, as the first J - V scan with thin TaTm HTL shows rather low V_{oc} and FF (Figure 1c).

However, with consecutive scans, the solar cell characteristics are recovered, indicating that charges which accumulate (during consecutive scans) at the ITO/TaTm interface reduce the energy barrier likely by doping of TaTm. When the TaTm thickness is further reduced (2 nm, Figure S2, Supporting Information), the dynamic behavior disappears. This fact could indicate a favorable band bending at the ITO/TaTm contact, making a thin HTL

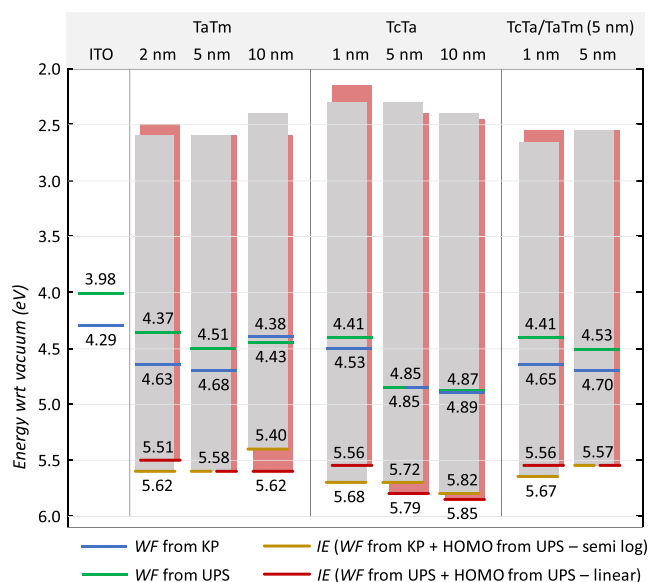


Figure 4. Summary of experimentally determined WF and IE for bare ITO, ITO coated with TaTm or TcTa (increasing thickness), and for bilayers of TcTa (1 and 5 nm) and TaTm (5 nm). WF is obtained from KP (blue lines) and UPS SECO (green lines). The IE is calculated in two ways: 1) from linear extrapolation of the UPS HOMO region and using the WF measured with UPS during the first scan (red lines); 2) from semi-log extrapolation of the UPS HOMO region and using the WF measured with KP. The HOMO–LUMO difference for TaTm (3.0 eV)^[24] and TcTa (3.4 eV)^[23] is represented as colored rectangles and adjusted to each estimated IE.

effectively behaving as a surface WF modifier, in analogy to SAMs. A similar mechanism can be envisioned for the TcTa/TaTm bilayer when the TcTa is only 1 nm thick, as the energy levels and J - V curves are similar to those of devices with thin TaTm. When the TcTa is thicker (5 nm) in the bilayer HTL, the s-shaped J - V curve (Figure 2a) indicates that the diode built-in potential is much lower than the V_{oc} .^[13,58] At this thickness, the WF and IE of TcTa are similar to those of its bulk (4.89 and 5.82 eV for 10 nm thick films, Figure 4), in agreement with previous reports.^[23] Hence, if the TcTa film is not thin enough, the energy barrier for hole transfer is even higher as compared to the case of 10 nm thick TaTm films, hindering charge injection/collection.

One of the most widely used polymer HTLs is PTAA (with an IE of approximately 5.1–5.2 eV),^[13,59] which is typically coated on top of ITO without any interlayer.^[60] It has been previously shown that the FF of solar cells is highly dependent on the PTAA thickness,^[61] and for this reason, the polymer is often doped by blending with p-dopants, such as (2,3,5,6-tetrafluoro-2,5-cyclohexadiene-1,4-diyldiene)dimalononitrile (F_4 -TCNQ).^[62] We have also tested thin PTAA layers (<10 nm) as HTL in our perovskite solar cells to check its performance, and especially the eventual appearance of dynamic behavior during consecutive J - V scans. As shown in Figure S8 in the Supporting Information, solar cells prepared on ITO/PTAA substrates exhibit similar behavior to those based on small-molecular-weight semiconductors presented earlier. With PTAA, we observed the V_{oc} and J_{sc} to be close to their maximum values from the first measurement, and the PCE evolution is dominated by the FF, which increases

with subsequent cycles to stabilize around 75%, leading to PCE of approximately 17.5%. These data suggest that for a generic HTL (either a small molecule or a polymer) to be suitable in p–i–n perovskite solar cells without the use of dopants or high WF interlayers, its IE should be close (within 0.1–0.2 eV) in energy to the VB edge of the perovskite, and the HTL should be thin enough to allow ohmic hole transfer at the electrode.

We finally studied the stability of the thin HTLs to check whether the benefit in terms of processability, avoiding the use of high WF interlayers, translates into device stability.

We initially tested the solar cells with TaTm (5 nm) and TcTa (1 nm)/TaTm (5 nm) bilayers as HTLs. The devices were encapsulated with a UV-curable resin and a glass slide, and the stability was evaluated in a nitrogen atmosphere to minimize the influences of extrinsic environmental factors on the degradation. To evaluate the operational stability, the devices were maintained at their MPP under simulated 1 sun equivalent illumination with white LEDs at room temperature (25 °C). Under these operational conditions, the time to reach 80% of the initial PCE (t_{80}) was approximately 500 h (Figure 5a), with no appreciable differences for the two types of HTLs, and in agreement with previous reports on similar device stacks, including an MoO₃ interlayer.^[50]

We further assessed the stability of these devices during thermal stress. For this, the solar cells were maintained at 65 °C (on a hot plate) at open circuit in the dark and in a nitrogen atmosphere. Periodically, the J - V characteristics under simulated 1 sun illumination were recorded at room temperature. As depicted in Figure 5b, the solar cells with 5 nm thick TaTm HTL were found to be thermally unstable, as even after 1 day at 65 °C, both V_{oc} and FF were strongly reduced, a degradation that continued throughout the duration of our experiment (6 days). Similar behavior was observed for the devices with TcTa (1 nm)/TaTm (5 nm) bilayer (Figure S9, Supporting Information). To understand the origin of this degradation, we also tested reference perovskite solar cells, employing a MoO₃ (5 nm)/TaTm (10 nm) p-type contact. Similar to the solar cells with the thin HTLs, they were also not thermally stable, with a strong reduction of the V_{oc} and FF in the first day at 65 °C (Figure 5c). Hence, the MoO₃ interlayer, which ensures ohmic contact at the ITO interface, does not provide benefits in terms of thermal stability. As a comparison, we also tested devices using PTAA as the HTL, which were the only ones stable at 65 °C for up to 12 days, with only a minor V_{oc} reduction after 1 day of thermal stress (Figure 5d). To cross-check the effect of MoO₃ on the stability of the stack, we also prepared devices with MoO₃/PTAA as p-type contact, which were found to be degraded even after 1 day of operation (Figure S10, Supporting Information), indicating that indeed MoO₃ is a cause of instability in p–i–n perovskite devices. In contrast, the reason why the thermal stability of devices with thin PTAA outperforms that of cells with TaTm is more difficult to rationalize, especially considering their similar chemical structure and related properties. High-molecular-weight PTAA has a glass transition temperature (T_g) of approximately 100 °C,^[63,64] which is very similar to other arylamine derivatives such as N,N' -bis(naphthalen-1-yl)- N,N' -bis(phenyl)-benzidine (NPB),^[65] whose structure is very close to TaTm. To double-check this point, we have also tested the thermal stability of perovskite solar cells with a thin layer of Spiro-TTB (5 nm), with a $T_g = 146$ °C.^[65] Despite this and an initial

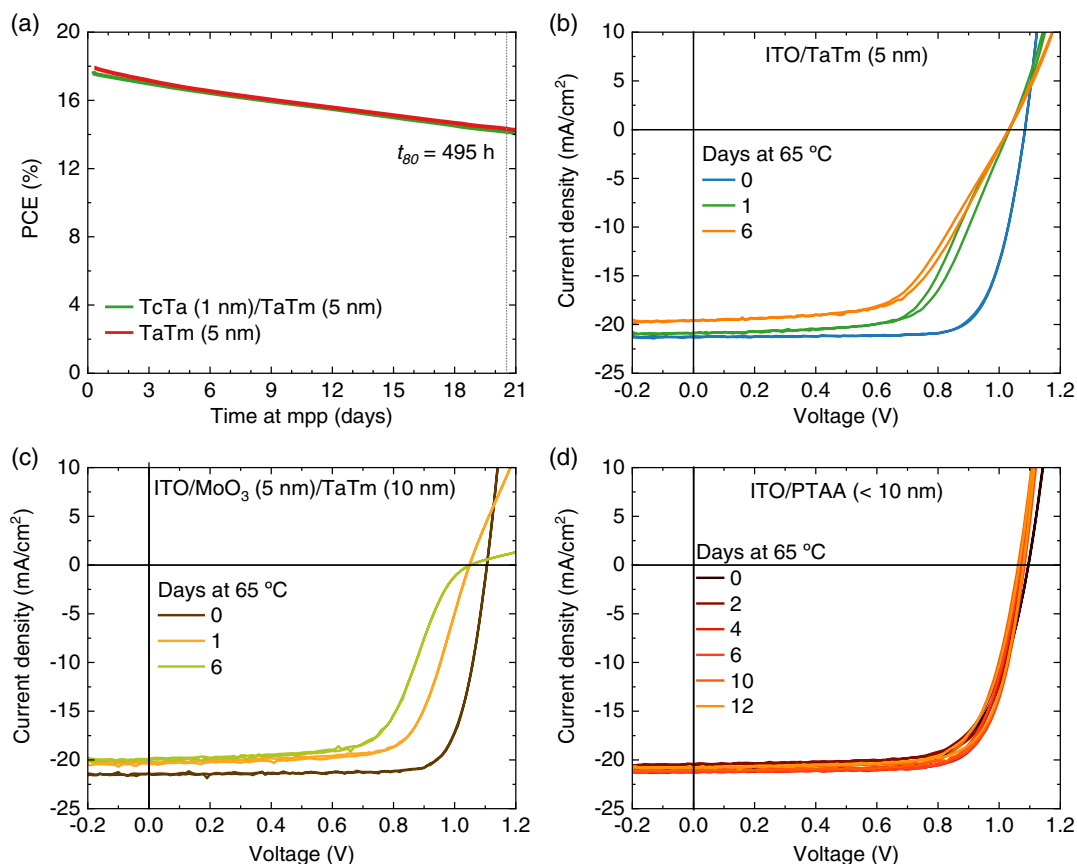


Figure 5. a) Continuous MPP tracking under simulated solar illumination for solar cells with TaTm and TcTa/TaTm as the HTL. J - V curves taken at different times for solar cells kept at 65 °C in a nitrogen atmosphere and with different HTLs: a) TaTm (5 nm), b) MoO₃ (5 nm)/TaTm (10 nm), and c) PTAA (<10 nm).

good PCE (>17%), the devices with this HTM were also found to be thermally unstable (Figure S11, Supporting Information). The thermal instability of solar cells, including small-molecule HTLs, might originate from other phenomena, for example, temperature-induced aggregation,^[66] which has been shown to readily occur in TcTa and NPB thin films at elevated temperatures.^[67] To test this hypothesis, we have studied the surface properties of thin TaTm films before and after annealing at 85 °C for several hours. X-ray photoemission spectroscopy of as-prepared and thermally stressed films reveals that no chemical changes (i.e., oxidation) occur during annealing of this small molecule (Figure S12, Supporting Information). The photoluminescence spectra of the TaTm films are also unaltered, independently of their thickness (Figure S13, Supporting Information). We observed a small change in surface morphology by atomic force microscopy (AFM, Figure S14, Supporting Information), with the annealed sample showing slightly larger aggregates and an increased RMS roughness ($R_{\text{RMS}} = 1.51$) compared to the as-deposited sample ($R_{\text{RMS}} = 1.26$). Small changes were also observed in the water contact angle (Figure S15, Supporting Information), increasing from 36°–37° to 40°–41° (decrease of surface energy) for the as-deposited and annealed sample, respectively. While the AFM and contact angle measurements show an evolution of the TaTm surface upon thermal stressing at 85 °C for 6 h, suggesting a rearrangement of the molecular

aggregation, these changes are small and unlikely to be the main reason for the device's thermal instability. We cannot exclude other chemical reactions or molecular diffusions between the HTL and the perovskite,^[68] which would also hinder device functioning. However, the HTL/perovskite is buried and hence of difficult access to analytical probes. Further detailed investigations are needed to clarify the origin of the thermal degradation of solar cells including small-molecule HTLs.

3. Conclusions

Thin films of intrinsic organic semiconductors were investigated as selective HTLs in fully vacuum-deposited perovskite solar cells. Different materials, both small molecules and polymers, can be used to make ohmic contacts at the interface between transparent electrodes (ITO) and the perovskite. For HTL thickness >5 nm, solar cells show a dynamic behavior during consecutive J - V scans, indicating the presence of an energy barrier at the ITO/HTL interface, which is slowly overcome until stabilization of the power output, likely as a consequence of (photo-)doping at the interface. Nevertheless, if the thickness is below 5 nm, good rectification (high FF) is immediately achieved. The surface electronic properties of the materials were studied by a combination of KP and UPS, revealing that the thin

HTLs effectively serve as WF enhancer, maintaining selective hole transport. We have studied the thermal stability of the perovskite solar cells and found that small molecules are, in general, not thermally stable, as opposed to the widely used polymer PTAA. The surface morphology and energy of TaTm were observed to change upon annealing, but the changes are not sufficient to identify molecular aggregation as a main driver for the device's instability. Thermal stress could also trigger chemical reactions and diffusion of species at the HTL/perovskite interface, undermining the device's functioning. These phenomena will be the topic of future studies, with the aim of establishing simple, efficient, and thermally stable interfaces for perovskite solar cells.

4. Experimental Section

Materials: TaTm was provided by Novald GmbH. Fullerene (C₆₀) and PTAA were purchased from Merck KGaA. PbI₂, CH₃NH₃I (MAI), MoO₃, BCP, TcTa, and Spiro-TTB were purchased from Luminescence Technology Corp. All materials were used as received.

Thin Film and Device Preparation: ITO-coated glass substrates were subsequently cleaned with soap, water, and isopropanol in an ultrasonic bath, followed by UV-ozone treatment. They were transferred to a vacuum chamber integrated into a nitrogen-filled glovebox (H₂O and O₂ < 0.1 ppm) and evacuated to a pressure of 10⁻⁶ mbar. All the layers were prepared by vacuum sublimation of the corresponding inorganic or organic materials using quartz crystal microbalance sensors to monitor the deposition rate. HTLs were sublimed with a deposition rate of 0.1 Å s⁻¹. The perovskite films were deposited in a second chamber by co-evaporation of MAI and PbI₂ precursors simultaneously at the rates of 1.0 and 0.6 Å s⁻¹, respectively. After deposition of a 500 nm thick perovskite film, the layer of C₆₀ (25 nm) and a thin layer of BCP (7 nm) were evaporated at a rate of 0.5 and 0.3 Å s⁻¹, respectively. To finish the device, the metal top contact Ag (100 nm) was sublimed in a third vacuum chamber.

Materials and Devices Characterization: The crystalline structure of the film samples was studied by XRD. The patterns were collected in Bragg-Brentano geometry on an Empyrean PANalytical powder diffractometer with a copper anode operated at 45 kV and 40 mA. Further analysis, including Le Bail fits, was performed with Fullprof software. SEM images were performed on a Hitachi S-4800 microscope operating at an accelerating voltage of 2 kV over platinum-metallized samples.

UPS measurements were performed in a UHV system with a base pressure of <1 × 10⁻¹⁰ mbar. The system was equipped with a Scienta-Omicron SES-100 electron analyzer and a UV source (He-I = 21.22 eV). All UPS spectra were corrected by mathematical subtraction of unwanted features from secondary He-I satellite emission lines (23.09 and 23.05 eV). Pass energy of 2 eV was used for UPS spectra. The electron analyzer was calibrated using a clean surface of the Au sample by measuring Fermi Energy (E_F = 0). Possible ultraviolet radiation damage or unwanted effects were monitored by performing the measurements as a set of consecutive scans for each region. Each scan took about 2 min. If no changes were observed in the scans, then it was averaged into one scan. All UPS samples were handled and transferred only in an inert atmosphere of nitrogen using UHV compatible suitcases and were never exposed to ambient air. UPS data processing was performed using Casa XPS 2.3.16 software.

CPD measurements using KP system (Besocke Delta Phi) were performed in a nitrogen-filled glovebox with H₂O and O₂ levels monitored and below 0.1 ppm. The KP system is equipped with a gold grid of 2.5 mm mounted on a piezoelectric drive with sensitivity <0.1 mV. The probe was operated with a standard vibration of about 160 Hz (time constant (t) of 1). The WF for each sample was measured several times and in different positions. A freshly cleaved HOPG (AGraphZ, mosaic spread 0.4° ± 0.1°, Optigraph) surface was used every time to calibrate the WF of the probe prior to each measurement. A reference value for the freshly cleaved HOPG surface of 4.475 eV was used.

The J–V curves for the solar cells were recorded using a Keithley 2612 A SourceMeter in a –0.2 and 1.3 V voltage range, with 0.01 V steps, and integrating the signal for 20 ms after a 10 ms delay, corresponding to a scan speed of about 0.3 V s⁻¹. The devices were illuminated under a Wavelabs Sinus 70 LED solar simulator. The light intensity was calibrated before every measurement using a calibrated Si reference diode (Abet Technologies, Inc.).

Solar cell stability measurements were taken using an MPP tracker system, with a white LED light source under 1 sun equivalent, developed by candlelight. The encapsulated devices were exposed to a flow of N₂ gas, while the temperature was maintained at 300 K during the entire measurement using a water-circulating cooling system controlled by a Peltier element, and J–V curve measurements were performed every 10 min.

Supporting Information

Supporting Information is available from the Wiley Online Library or from the author.

Acknowledgements

The authors acknowledge the funding from the Ministry of Science and Innovation (MCIN) and the Spanish State Research Agency (AEI). Project RTI2018-095362-A-I00 was funded by MCIN/AEI/10.13039/501100011033 and “ERDF A way of making Europe.” Project PCI2020-112084 was funded by MCIN/AEI/10.13039/501100011033 and the “European Union NextGenerationEU/PRTR.” Grant RYC-2016-21316 was funded by MCIN/AEI/10.13039/501100011033 and “ESF Investing in your future.” The work was carried out in the framework of the SOLAR-ERA.NET project PERDRY, for which Z.H. and E.M. acknowledge the financial support from the Swedish Energy Council (Energimyndigheten, contract 48381-1). E.M. acknowledges the Knut and Alice Wallenberg Foundation (Grant KAW-2016-0059) for financial support of the research group and the Carl Trygger Foundation (grant CTS15: 332) for funding the KP set-up. The authors thank Leif K.E. Ericsson for invaluable technical support with the KP and UPS equipment.

Conflict of Interest

The authors declare no conflict of interest.

Data Availability Statement

The data that support the findings of this study are available from the corresponding author upon reasonable request.

Keywords

doping, hole transport layers, organic semiconductors, perovskite solar cells, small molecules

Received: October 21, 2021

Revised: December 5, 2021

Published online:

- [1] A. Kojima, K. Teshima, Y. Shirai, T. Miyasaka, *J. Am. Chem. Soc.* **2009**, *131*, 6050.
- [2] W. A. Dunlap-Shohl, Y. Zhou, N. P. Padture, D. B. Mitzi, *Chem. Rev.* **2019**, *119*, 3193.
- [3] M. Saliba, J. P. Correa-Baena, M. Grätzel, A. Hagfeldt, A. Abate, *Angew. Chem., Int. Ed.* **2018**, *57*, 2554.

- [4] M. A. Green, E. D. Dunlop, J. Hohl-Ebinger, M. Yoshita, N. Kopidakis, X. Hao, *Prog. Photovoltaics Res. Appl.* **2021**, *29*, 657.
- [5] M. Jeong, I. W. Choi, E. M. Go, Y. Cho, M. Kim, B. Lee, S. Jeong, Y. Jo, H. W. Choi, J. Lee, J.-H. Bae, S. K. Kwak, D. S. Kim, C. Yang, *Science* **2020**, *369*, 1615.
- [6] Y. Rong, Y. Hu, A. Mei, H. Tan, M. I. Saidaminov, S. Il Seok, M. D. McGehee, E. H. Sargent, H. Han, *Science* **2018**, *361*, eaat8235.
- [7] Z. Song, C. L. McElvany, A. B. Phillips, I. Celik, P. W. Krantz, S. C. Waththage, G. K. Liyanage, D. Apul, M. J. Heben, *Energy Environ. Sci.* **2017**, *10*, 1297.
- [8] H. S. Jung, N. G. Park, *Small* **2015**, *11*, 10.
- [9] J. Jeong, M. Kim, J. Seo, H. Lu, P. Ahlawat, A. Mishra, Y. Yang, M. A. Hope, F. T. Eickemeyer, M. Kim, Y. J. Yoon, I. W. Choi, B. P. Darwich, S. J. Choi, Y. Jo, J. H. Lee, B. Walker, S. M. Zakeeruddin, L. Emsley, U. Rothlisberger, A. Hagfeldt, D. S. Kim, M. Grätzel, J. Y. Kim, *Nature* **2021**, *592*, 381.
- [10] X. Zheng, Y. Hou, C. Bao, J. Yin, F. Yuan, Z. Huang, K. Song, J. Liu, J. Troughton, N. Gasparini, C. Zhou, Y. Lin, D.-J. Xue, B. Chen, A. K. Johnston, N. Wei, M. N. Hedhili, M. Wei, A. Y. Alsalloum, P. Maity, B. Tureddi, C. Yang, D. Baran, T. D. Anthopoulos, Y. Han, Z.-H. Lu, O. F. Mohammed, F. Gao, E. H. Sargent, O. M. Bakr, *Nat. Energy* **2020**, *5*, 131.
- [11] H. D. Pham, L. Xianqiang, W. Li, S. Manzhos, A. K. K. Kyaw, P. Sonar, *Energy Environ. Sci.* **2019**, *12*, 1177.
- [12] W. Yan, S. Ye, Y. Li, W. Sun, H. Rao, Z. Liu, Z. Bian, C. Huang, *Adv. Energy Mater.* **2016**, *6*, 1600474.
- [13] M. Stollerfoht, P. Caprioglio, C. M. Wolff, J. A. Márquez, J. Nordmann, S. Zhang, D. Rothhardt, U. Hörmann, Y. Amir, A. Redinger, L. Kegelmann, F. Zu, S. Albrecht, N. Koch, T. Kirchartz, M. Saliba, T. Unold, D. Neher, *Energy Environ. Sci.* **2019**, *12*, 2778.
- [14] P. Schulz, D. Cahen, A. Kahn, *Chem. Rev.* **2019**, *119*, 3349.
- [15] Z. Hawash, L. K. Ono, Y. Qi, *Adv. Mater. Interfaces* **2018**, *5*, 1700623.
- [16] W. S. Yang, B. W. Park, E. H. Jung, N. J. Jeon, Y. C. Kim, D. U. Lee, S. S. Shin, J. Seo, E. K. Kim, J. H. Noh, S. Il Seok, *Science* **2017**, *356*, 1376.
- [17] W. Chen, Y. Wu, Y. Yue, J. Liu, W. Zhang, X. Yang, H. Chen, E. Bi, I. Ashraf, M. Grätzel, L. Han, *Science* **2015**, *350*, 944.
- [18] F. Hou, Z. Su, F. Jin, X. Yan, L. Wang, H. Zhao, J. Zhu, B. Chu, W. Li, *Nanoscale* **2015**, *7*, 9427.
- [19] T. Liu, D. Kim, H. Han, A. R. Bin Mohd Yusoff, J. Jang, *Nanoscale* **2015**, *7*, 10708.
- [20] O. Malinkiewicz, A. Yella, Y. H. Lee, G. M. Espallargas, M. Graetzel, M. K. Nazeeruddin, H. J. Bolink, *Nat. Photonics* **2014**, *8*, 128.
- [21] T. H. Schloemer, J. A. Christians, J. M. Luther, A. Sellinger, *Chem. Sci.* **2019**, *10*, 1904.
- [22] S. S. Shin, S. J. Lee, S. Il Seok, *Adv. Funct. Mater.* **2019**, *29*, 1900455.
- [23] N. B. Kotadiya, H. Lu, A. Mondal, Y. Ie, D. Andrienko, P. W. M. Blom, G. J. A. H. Wetzelaer, *Nat. Mater.* **2018**, *17*, 329.
- [24] C. Momblona, L. Gil-Escrig, E. Bandiello, E. M. Hutter, M. Sessolo, K. Lederer, J. Blochwitz-Nimoth, H. J. Bolink, *Energy Environ. Sci.* **2016**, *9*, 3456.
- [25] J. Avila, L. Gil-Escrig, P. P. Boix, M. Sessolo, S. Albrecht, H. J. Bolink, *Sustainable Energy Fuels* **2018**, *2*, 2429.
- [26] M. Kröger, S. Hamwi, J. Meyer, T. Riedl, W. Kowalsky, A. Kahn, *Appl. Phys. Lett.* **2009**, *95*, 123301.
- [27] P. Schulz, J. O. Tjepelt, J. A. Christians, I. Levine, E. Edri, E. M. Sanehira, G. Hodes, D. Cahen, A. Kahn, *ACS Appl. Mater. Interfaces* **2016**, *8*, 31491.
- [28] A. Babaei, K. P. S. Zanon, L. Gil-Escrig, D. Pérez-del-Rey, P. P. Boix, M. Sessolo, H. J. Bolink, *Front. Chem.* **2020**, *7*, 1.
- [29] T. H. Schloemer, J. A. Raiford, T. S. Gehan, T. Moot, S. Nanayakkara, S. P. Harvey, R. C. Bramante, S. Dunfield, A. E. Louks, A. E. Maughan, L. Bliss, M. D. McGehee, M. F. A. M. van Hest, M. O. Reese, S. F. Bent, J. J. Berry, J. M. Luther, A. Sellinger, *ACS Energy Lett.* **2020**, *5*, 2349.
- [30] D. Bi, G. Boschloo, A. Hagfeldt, *Nano* **2014**, *09*, 1440001.
- [31] S. Ryu, J. Seo, S. S. Shin, Y. C. Kim, N. J. Jeon, J. H. Noh, S. Il Seok, *J. Mater. Chem. A* **2015**, *3*, 3271.
- [32] J.-P. Correa-Baena, W. Tress, K. Domanski, E. H. Anaraki, S.-H. Turren-Cruz, B. Roose, P. P. Boix, M. Grätzel, M. Saliba, A. Abate, A. Hagfeldt, *Energy Environ. Sci.* **2017**, *10*, 1207.
- [33] D. Zhao, M. Sexton, H.-Y. Park, G. Baure, J. C. Nino, F. So, *Adv. Energy Mater.* **2015**, *5*, 1401855.
- [34] K. Tvingstedt, L. Gil-Escrig, C. Momblona, P. Rieder, D. Kiermasch, M. Sessolo, A. Baumann, H. J. Bolink, V. Dyakonov, *ACS Energy Lett.* **2017**, *2*, 424.
- [35] Z. Liu, L. Krückemeier, B. Krogmeier, B. Klingebiel, J. A. Márquez, S. Levchenko, S. Öz, S. Mathur, U. Rau, T. Unold, T. Kirchartz, *ACS Energy Lett.* **2019**, *4*, 110.
- [36] M. Stollerfoht, C. M. Wolff, J. A. Márquez, S. Zhang, C. J. Hages, D. Rothhardt, S. Albrecht, P. L. Burn, P. Meredith, T. Unold, D. Neher, *Nat. Energy* **2018**, *3*, 847.
- [37] A. Al-Ashouri, A. Magomedov, M. Roß, M. Jošt, M. Talaikis, G. Chistiakova, T. Bertram, J. A. Márquez, E. Köhnen, E. Kasparavičius, S. Levchenko, L. Gil-Escrig, C. J. Hages, R. Schlattmann, B. Rech, T. Malinauskas, T. Unold, C. A. Kaufmann, L. Korte, G. Niaura, V. Getautis, S. Albrecht, *Energy Environ. Sci.* **2019**, *12*, 3356.
- [38] Z. Dai, S. K. Yadavalli, M. Chen, A. Abbaspourtamijani, Y. Qi, N. P. Padture, *Science* **2021**, *372*, 618.
- [39] J. Ávila, C. Momblona, P. P. Boix, M. Sessolo, H. J. Bolink, *Joule* **2017**, *1*, 431.
- [40] R. Swartwout, M. T. Hoerantner, V. Bulović, *Energy Environ. Mater.* **2019**, *2*, 119.
- [41] Y. Vaynzof, *Adv. Energy Mater.* **2020**, *10*, 2003073.
- [42] M. Roß, L. Gil-Escrig, A. Al-Ashouri, P. Tockhorn, M. Jošt, B. Rech, S. Albrecht, *ACS Appl. Mater. Interfaces* **2020**, *12*, 39261.
- [43] M. Roß, S. Severin, M. B. Stutz, P. Wagner, H. Köbler, M. Favini-Lévêque, A. Al-Ashouri, P. Korb, P. Tockhorn, A. Abate, B. Stannowski, B. Rech, S. Albrecht, *Adv. Energy Mater.* **2021**, *11*, 2101460.
- [44] T. Abzieher, T. Feeney, F. Schackmar, Y. J. Donie, I. M. Hossain, J. A. Schwenzler, T. Hellmann, T. Mayer, M. Powalla, U. W. Paetzold, *Adv. Funct. Mater.* **2021**, *31*, 2104482.
- [45] S. Olthof, K. Meerholz, *Sci. Rep.* **2017**, *7*, 40267.
- [46] D. Pérez-del-Rey, P. P. Boix, M. Sessolo, A. Hadipour, H. J. Bolink, *J. Phys. Chem. Lett.* **2018**, *9*, 1041.
- [47] T. Abzieher, S. Moghadamzadeh, F. Schackmar, H. Eggers, F. Sutterlütli, A. Farooq, D. Kojda, K. Habicht, R. Schmager, A. Mertens, R. Azmi, L. Klöhr, J. A. Schwenzler, M. Hetterich, U. Lemmer, B. S. Richards, M. Powalla, U. W. Paetzold, *Adv. Energy Mater.* **2019**, *9*, 1802995.
- [48] Y. Choi, D. Koo, M. Jeong, G. Jeong, J. Lee, B. Lee, K. J. Choi, C. Yang, H. Park, *Sol. RRL* **2021**, *5*, 2100415.
- [49] F. Palazon, D. Pérez-del-Rey, B. Dänekamp, C. Dreessen, M. Sessolo, P. P. Boix, H. J. Bolink, *Adv. Mater.* **2019**, *31*, 1902692.
- [50] A. Babaei, C. Dreessen, M. Sessolo, H. J. Bolink, *RSC Adv.* **2020**, *10*, 6640.
- [51] E. E. Looney, Z. Liu, A. Classen, H. Liu, N. Riedel, M. Braga, P. Balaji, A. Augusto, T. Buonassisi, I. Marius Peters, *Prog. Photovoltaics Res. Appl.* **2021**, *29*, 200.
- [52] R. Schlaf, H. Murata, Z. Kafafi, *J. Electron Spectrosc. Relat. Phenomena* **2001**, *120*, 149.
- [53] M. G. Helander, M. T. Greiner, Z. B. Wang, Z. H. Lu, *Appl. Surf. Sci.* **2010**, *256*, 2602.
- [54] X. Crispin, *Sol. Energy Mater. Sol. Cells* **2004**, *83*, 147.

- [55] Z. Hu, Z. Zhong, K. Zhang, Z. Hu, C. Song, F. Huang, J. Peng, J. Wang, Y. Cao, *NPG Asia Mater.* **2017**, *9*, e379.
- [56] P. Schulz, E. Edri, S. Kirmayer, G. Hodes, D. Cahen, A. Kahn, *Energy Environ. Sci.* **2014**, *7*, 1377.
- [57] J. Endres, D. A. Egger, M. Kulbak, R. A. Kerner, L. Zhao, S. H. Silver, G. Hodes, B. P. Rand, D. Cahen, L. Kronik, A. Kahn, *J. Phys. Chem. Lett.* **2016**, *7*, 2722.
- [58] W. Tress, K. Leo, M. Riede, *Adv. Funct. Mater.* **2011**, *21*, 2140.
- [59] W. Zhang, J. Smith, R. Hamilton, M. Heeney, J. Kirkpatrick, K. Song, S. E. Watkins, T. Anthopoulos, I. McCulloch, *J. Am. Chem. Soc.* **2009**, *131*, 10814.
- [60] F. M. Rombach, S. A. Haque, T. J. Macdonald, *Energy Environ. Sci.* **2021**, *14*, 5161.
- [61] V. M. Le Corre, M. Stolterfoht, L. Perdigón Toro, M. Feuerstein, C. Wolff, L. Gil-Escrig, H. J. Bolink, D. Neher, L. J. A. Koster, *ACS Appl. Energy Mater.* **2019**, *2*, 6280.
- [62] Q. Wang, C. Bi, J. Huang, *Nano Energy* **2015**, *15*, 275.
- [63] S. Barard, M. Heeney, L. Chen, M. Cölle, M. Shkunov, I. McCulloch, N. Stingelin, M. Philips, T. Kreouzis, *J. Appl. Phys.* **2009**, *105*, 013701.
- [64] A. Intaniwet, C. A. Mills, M. Shkunov, H. Thiem, J. L. Keddie, P. J. Sellin, *J. Appl. Phys.* **2009**, *106*, 064513.
- [65] C. Murawski, C. Fuchs, S. Hofmann, K. Leo, M. C. Gather, *Appl. Phys. Lett.* **2014**, *105*, 113303.
- [66] B. Du, J. Yi, H. Yan, T. Wang, *Chem. – A Eur. J.* **2021**, *27*, 2908.
- [67] H.-K. Choi, S.-H. Lee, Y.-J. Lim, S.-T. Lee, J.-H. Lee, J.-H. Lee, *AIP Adv.* **2020**, *10*, 065226.
- [68] Z. Ahmad, A. Mishra, S. M. Abdulrahim, D. Taguchi, P. Sanghyun, F. Aziz, M. Iwamoto, T. Manaka, J. Bhadra, N. J. Al-Thani, M. K. Nazeeruddin, F. Touati, A. Belaidi, S. A. Al-Muhtaseb, *Sci. Rep.* **2021**, *11*, 33.